JOURNAL OF GEOPHYSICAL RESEARCH, VOL. 116, C03013, doi:10.1029/2010JC006557, 2011

Discovery of a natural CO_2 seep in the German North Sea: Implications for shallow dissolved gas and seep detection

Daniel F. McGinnis,[1] Mark Schmidt,[1] Tonya DelSontro,[2] Sören Themann,[3]
Lorenzo Rovelli,[1] Anja Reitz,[1] and Peter Linke[1]

Received 27 July 2010; revised 23 November 2010; accepted 14 December 2010; published 5 March 2011.

[1] A natural carbon dioxide (CO_2) seep was discovered during an expedition to the southern German North Sea (October 2008). Elevated CO_2 levels of ~10–20 times above background were detected in seawater above a natural salt dome ~30 km north of the East-Frisian Island Juist. A single elevated value 53 times higher than background was measured, indicating a possible CO_2 point source from the seafloor. Measured pH values of around 6.8 support modeled pH values for the observed high CO_2 concentration. These results are presented in the context of CO_2 seepage detection, in light of proposed subsurface CO_2 sequestering and growing concern of ocean acidification. We explore the boundary conditions of CO_2 bubble and plume seepage and potential flux paths to the atmosphere. Shallow bubble release experiments conducted in a lake combined with discrete-bubble modeling suggest that shallow CO_2 outgassing will be difficult to detect as bubbles dissolve very rapidly (within meters). Bubble-plume modeling further shows that a CO_2 plume will lose buoyancy quickly because of rapid bubble dissolution while the newly CO_2-enriched water tends to sink toward the seabed. Results suggest that released CO_2 will tend to stay near the bottom in shallow systems (<200 m) and will vent to the atmosphere only during deep water convection (water column turnover). While isotope signatures point to a biogenic source, the exact origin is inconclusive because of dilution. This site could serve as a natural laboratory to further study the effects of carbon sequestration below the seafloor.

Citation: McGinnis, D. F., M. Schmidt, T. DelSontro, S. Themann, L. Rovelli, A. Reitz, and P. Linke (2011), Discovery of a natural CO_2 seep in the German North Sea: Implications for shallow dissolved gas and seep detection, *J. Geophys. Res.*, *116*, C03013, doi:10.1029/2010JC006557.

1. Introduction

1.1. General Background

[2] The most significant carbon dioxide (CO_2) emission to the atmosphere is from burning fossil fuels and deforestation [*Intergovernmental Panel on Climate Change* (*IPCC*), 2007]. The importance of the oceans, particularly the coastal shelf seas, as sources and sinks for atmospheric CO_2 is subsequently an area of increasing focus [*Siegenthaler and Sarmiento*, 1993; *Kennett et al.*, 2003; *Sabine et al.*, 2004; *Friedrich and Oschlies*, 2009]. The oceans are a principal sink for anthropogenic atmospheric CO_2; however, rising CO_2 concentrations are estimated to have caused a 30% increase in the concentration of H^+ in ocean surface waters since the early 1900s and may lead to a drop in seawater pH of up to 0.5 units by 2100 [*Siegenthaler and Sarmiento*, 1993; *Caldeira and Wickett*, 2005; *IPCC*, 2007].

[3] To mitigate the effects on ocean acidification and climate forcing, CCS (carbon capture and storage), in which point source CO_2 emissions are captured and sequestered within the geosphere, has been extensively proposed [e.g., *Lenton and Cannel*, 2002; *Haugan and Joos*, 2004; *Haszeldine*, 2009; *Orr*, 2009; *Schrag*, 2009]. Some proponents argue that CCS below the seafloor has the advantage of the overlying water acting as a buffer in case of accidental or unexpected leakage. However, there is concern and little known about the impact of leakage on local ecosystems, the potential of CO_2 interaction liberating toxic substances (e.g., heavy metals), or the potential for seepage to vent to the atmosphere (bubbles, plumes, etc.) [*Leifer and Patro*, 2002; *Dimitrov*, 2003; *Holloway et al.*, 2007; *Kharaka et al.*, 2006].

[4] While many studies have been devoted to investigating methane (CH_4) seabed release [e.g., *Reeburgh*, 2003, 2007; *Keir et al.*, 2005, 2008; *Judd and Hovland*, 2007; and references therein], very little is known about natural CO_2 seepage, especially from sedimentary settings on continental shelves. In fact, with the exception of the natural CO_2 gas venting at Panarea (Aeolian Islands, Italy) [*Esposito et al.*,

[1]Leibniz Institute of Marine Sciences at University of Kiel (IFM-GEOMAR), Kiel, Germany.
[2]Surface Waters—Research and Management, Eawag: Swiss Federal Institute of Aquatic Science and Technology, Kastanienbaum, Switzerland.
[3]Sedimentology, Coastal- and Continental Shelf Research, Institute of Geosciences, University of Kiel, Kiel, Germany.

0148-0227/11/2010JC006557

2006], there are few studies at natural shallow CO_2 bubbling sites in the ocean. Natural CO_2 seepage is commonly found in CO_2-prone geological provinces, for example, in sedimentary basins at carbonated springs and mofettes or in volcanic and hydrothermal areas [*Dando et al.*, 2000; *Holloway et al.*, 2007; *Lewicki et al.*, 2007]. While natural CO_2 fluxes from volcanic vents and high-flow areas amount to less than 0.5% of anthropogenic emissions, these releases can alter local ocean geochemistry [*Hall-Spencer et al.*, 2008]. While most naturally occurring CO_2 originates from degassing magma, it can also be produced by metamorphism or dissolution of carbonate rocks, and thermal alteration or biodegradation of organic matter [e.g., *Berner*, 1980; *Ague*, 2000; *Fischer et al.*, 2006].

[5] The subsurface-produced CO_2 is typically emitted through the seabed as bubbles or enriched fluid [e.g., *Lupton et al.*, 2006; *Hall-Spencer et al.*, 2008]. In general, seepage from the seafloor is intermittent in response to hydrostatic pressure changes [*Tivey et al.*, 2002; *Linke et al.*, 2010; *Schneider von Deimling et al.*, 2010] and commonly produces pockmarks or other seabed expressions [e.g., *Judd and Hovland*, 2007; *Cathles et al.*, 2010]. If there are sufficient bubbles, then the induced buoyancy can create an upwelling of water together with the gas (bubble plume) [*Italiano and Nuccio*, 1991; *Linke et al.*, 2010]. Besides the obvious concern of CO_2 as a greenhouse gas, leaked CO_2 will decrease the pH of the water in the vicinity of the gas plume and increase its density, resulting in the tendency of CO_2-rich water to remain at or sink to the seafloor [*Ohsumi et al.*, 1992; *Haugan et al.*, 1995; *Alendal and Drange*, 2001]. Such conditions could potentially bleach corals and alter local flora or fauna [*Orr et al.*, 2005; *Hall-Spencer et al.*, 2008; *Veron et al.*, 2009]. Determining emissions and flux pathways from natural CO_2 seeps can provide estimates of the local risks and impacts, as well as the potential to reach the atmosphere. This knowledge can then be extrapolated to proposed or active anthropogenic CO_2 (CCS) storage sites [*Lewicki et al.*, 2007].

1.2. The North Sea as a "Continental Shelf Pump"

[6] As a net sink, the North Sea has been proposed to act as a "continental shelf pump" for atmospheric CO_2. It is suggested that ~93% of the atmospheric CO_2 absorbed by the surface waters is then transported to the North Atlantic Ocean where it is potentially sequestered within the interior [*Thomas et al.*, 2004; *Bozec et al.*, 2005]. *Thomas et al.* [2007], however, found that the CO_2 buffering capacity of the North Sea is diminishing as the surface water pCO_2 has increased (22 μatm increase from 2001 to 2005) twice as fast as the atmospheric pCO_2 (11 μatm) in the same period.

[7] While the water column experiences seasonal stratification in the north and central sections of the North Sea, the southern North Sea is vertically well mixed year round because of the shallow depth and strong currents [*Thomas et al.*, 2004; *Bozec et al.*, 2005; *Prowe et al.*, 2009]. With respect to CO_2 fluxes, the central and north (and largest) portions of the North Sea (north of the 54° parallel) act as a strong sink. However, the southern North Sea and English Channel are generally sources of CO_2. *Prowe et al.* [2009] estimate that 0.78 mol C m^{-2} yr^{-1} of CO_2 is released on an annual basis from the southern North Sea, while *Bozec et al.* [2005] report values from 0.8–1.7 mmol m^{-2} d^{-1}. *Prowe et al.* [2009] suggest that CO_2 fluxes increase in September up to 20 to 50 mmol m^{-2} d^{-1} with ΔpCO_2 values approaching 100 ppm. *Bozec et al.* [2005] also reported that the highest pCO_2 concentrations (400–450 μatm), compared to atmospheric values of 365 μatm, were found in the German Bight and English Channel water columns. They explain such high concentrations as being due to the mixing regime; however, the sources of CO_2 in the southern North Sea remain unknown.

1.3. Study Approach

[8] During a recent cruise to the southern German North Sea (Figure 1), we discovered elevated CO_2 values at the shallow (~30 m) study site, Salt Dome Juist, with values ranging from ~10–20 times above background, and a peak of >53 times above background (7000 μatm or ~300 μmol L^{-1}). We attribute these elevated concentrations to a natural CO_2 seep from a suspected biogenic source.

[9] In the context of CO_2 seep detection related to CCS, we present these findings of CO_2 emission in conjunction with modeling results demonstrating the expected seepage boundary conditions and projected flux paths to the atmosphere. Along with bubble release experiments conducted in Lake Lucerne (Switzerland), we show that CO_2 bubbles dissolve very rapidly in the sediment and the water column (within meters from the bottom) and compare CO_2 versus CH_4 bubble plume behavior. We anticipate that Salt Dome Juist and similar sites will serve as natural analogs to study ocean acidification and CO_2 seep detection at the ecosystem and geoengineering level in view of planned CCS sites in the North Sea [*Blackford et al.*, 2008].

2. Study Site and Methods

[10] Within the framework of the industry-founded project "Fluid and gas seepage in the southern German North Sea" (SDNS), an expedition onboard R/V *Alkor* (8–29 October 2008) was carried out to detect and map sediment gas and fluid migration pathways and to quantify gas fluxes and analyze their chemical composition. Bubble release experiments were conducted at Lake Lucerne (Switzerland) to compare the acoustic detection signal and rise behavior of CH_4 and CO_2 bubbles.

2.1. Study Site Geology

[11] Salt Dome Juist is located in the southern North Sea about 30 km offshore the East Frisian Island Juist, Germany (Figure 1). The Pleistocene and Holocene shelf architecture of this area is mainly affected by three extensive glaciations [*Ehlers*, 1990]. Consequently, repeated changes from glacial, periglacial, terrestrial and marine periods have formed a system of deep, Quaternary valleys and depressions [*Huuse and Lykke-Andersen*, 2000]. These structures have been filled with Pleistocene-aged organic rich deposits (e.g., peats and lignites) during a period of rising sea level. Decomposition of the organic matter subsequently led to the accumulation of shallow gas [*Streif*, 2002]. Deep seismic exploration in this area has revealed a complex structure of salt diapirism and tectonic faults in the deeper sediment strata [*Schroot and Schüttenhelm*, 2003]. These structures were created during the late Paleozoic and reach the seafloor

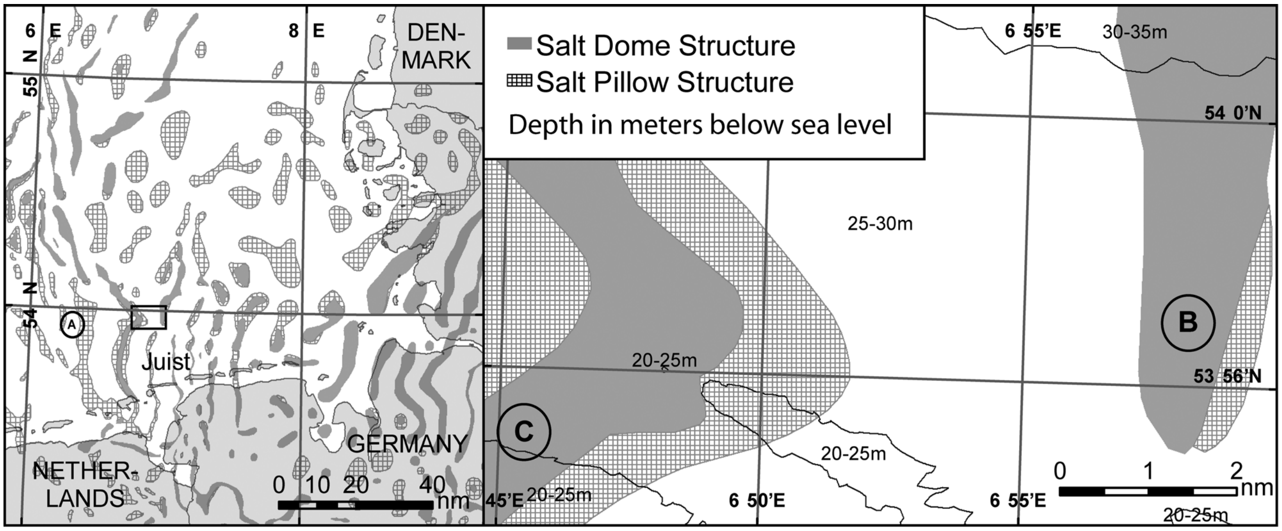

Figure 1. (left) Overview of study site (black box) in the southern North Sea and location of salt dome and pillow structures [*Lokhorst*, 1998]. (right) Detailed study site indicating CTD locations and depth contours. Area A, CTD 1 (reference); area B, CTDs 12, 15; area C, CTDs 13–14, 16.

in certain areas. Surface sediments in the region of Salt Dome Juist show a homogenous distribution of predominantly fine to medium coarse sands with shell fragments.

2.2. Onboard Equipment

[12] A 600 kHz acoustic Doppler current profiler (ADCP; Workhorse Monitor; Teledyne RDI Instruments, Poway, USA) was mounted downward looking in R/V *Alkor*'s moon pool ~1.5 m below the sea surface in standard profiling mode (Mode 5) with bottom tracking. The vertical bin size was set to 0.5 m for a total of 60 bins with a blanking distance of 1.12 m (range was therefore ~33 m). The ADCP tracks were simultaneously logged from the NMEA ship data. In addition to measuring current speed and direction, the ADCP measures individual beam backscatter which shows areas of increased turbidity and potentially indicates the presence of bubbles.

[13] Water column measurements were performed and water samples collected simultaneously with a SBE911plus conductivity-temperature-depth (CTD) profiler equipped with a 12 bottle rosette carousel (Sea-Bird Electronics, Inc., Washington, USA). The CTD sampled at 24 Hz and was also equipped with an O_2 sensor (dissolved oxygen), altimeter, and ship NMEA coordinate integration. As the water column was well mixed during our expedition, the CTD was towed several meters above the seafloor to search for constituent anomalies associated with seepage. Towed CTD casts were conducted with the ship drifting and the data were read online. The Niskin bottles were triggered when CTD anomalies were observed (e.g., spikes in temperature or conductivity). Bottle sample intervals typically ranged from about 10–100 m horizontally along the drift track. A total of 164 gas samples were obtained from 15 CTD/water sampling tracks in the Salt Dome Juist area.

[14] Dissolved gases were extracted from the sampled seawater by transferring 1.8 L of seawater from the Niskin bottle into a preevacuated gas-tight 2 L glass bottle directly after recovery [*Keir et al.*, 2008]. After temperature equilibration at laboratory conditions the gas phase was recompressed into 20 mL headspace vials at atmospheric pressure. The gas tight headspace vials were stored for further quantification and stable isotope measurements. This method has a proven >90% efficiency in extracting physically dissolved gases from seawater [*Keir et al.*, 2009]. Although the method used for degassing water samples is not an established method for determining pCO_2 and $\delta^{13}C\text{-}CO_2$, we will present the data here as qualitative results. Degassing of water samples at comparable temperatures was performed at about 18 ± 1°C and salinities of 34 ± 0.5 ‰. Moreover, kinetic isotope fractionation between gaseous CO_2 and dissolved CO_2 can be neglected during degassing processes [*Usdowski and Hoefs*, 1990]. Hence we assume that concentration and stable isotope values of extractable CO_2 ($CO_{2(extr.)}$) reflect the in situ CO_2 composition which provides good comparability of $CO_{2(extr.)}$ for the different sampling sites. CO_2 concentrations were measured by gas chromatography using a GC800top (CE Instruments, PorapackQ-MS5A combination, He-carrier gas, 50°C isotherm, HCD). The $\delta^{13}C$ values of $CO_{2(extr.)}$ were measured with a Delta Plus Advantage combined with a Gas Bench II inlet system (Thermo Finnigan). Isotope ratios are given in the δ notation versus Vienna Pee Dee Belemnite (VPDB) standard. Reproducibility of stable carbon isotope determination is about ±0.3 ‰.

[15] The program CO2SYS was used to calculate equilibrium $CO_{2(aq)}$ concentrations of between 6 to 13 μmol L^{-1} (T = 15°C, pH = 8.2–8.4, Alk = 2.4 meq L^{-1}) [*Pierrot et al.*, 2006].

2.3. Lake Lucerne Bubble Experiment

[16] A bubble measurement lander system was deployed at 12.5 m depth in a small boat harbor in Lake Lucerne (Switzerland). The system produced CO_2 bubbles (5000 ppm, CO_2 3.0 of Linde AG) of various sizes and was equipped with an online video recorder. We attached the CO_2 tank and pressure-compensated regulator, gas tight tubing, and a straight tube

fitting (Swagelok) directly to the lander frame. The bubble orifice was placed in the view of the underwater SuperSeaCam video camera (D6000, Deepsea Power and Light, San Diego, CA, USA) recording at 30 frames per second. The camera was connected via an underwater cable to the SuperSeaCam rack mount controller (S/N 104, Deepsea Power and Light, San Diego, CA, USA), which was used to zoom and focus from the surface. The video was recorded using Dazzle Video Creator Platinum (DVC107, Pinnacle Systems, Avid Technology) and images were analyzed in ImageJ (National Institutes of Health, USA). CO_2 bubbles released from the lander were recorded by a Simrad split-beam echosounder (EK60, 7° beam angle) with a 120 kHz transducer operating at a rate of 5 pings s^{-1}. The transducer was mounted to a small boat dock ~30 cm below the water surface and ~12 m directly above the lander. The echosounder was calibrated with a 23 mm diameter standard copper target [*Foote et al.*, 1987] and all data were recorded using Simrad ER60 software.

3. Bubble and Plume Modeling

3.1. Discrete Bubble Model

[17] The fate of CO_2 bubbles within and released from the sediment was modeled using a discrete bubble model (DBM) [*McGinnis and Little*, 2002; *McGinnis et al.*, 2006]. The behavior was then compared to that of CH_4 bubbles [*Ostrovsky et al.*, 2008]. The discrete bubble model predicts gas transfer (both dissolution and stripping) of five gaseous and dissolved species simultaneously (Ar, CO_2, CH_4, N_2, O_2). For a simple, stationary bubble (i.e., a bubble within the sediment), the equation is given as

$$\frac{dM_i}{dt} = -K_{Li}(H_iP_i - C_i)A_S, \tag{1}$$

which describes the rate of mass transfer in both directions across the bubble surface, where K_{Li} (m s^{-1}) is the liquid-side mass transfer coefficient of species i, A_S is the bubble surface area (m^2), and C_i is the dissolved concentration (mol m^{-3}). The local saturation concentration is given by the product of Henry's law constant H_i (mol m^{-3} Pa^{-1}) and partial pressure of gas within the bubble P_i (Pa), which largely controls the rate of dissolution or stripping.

[18] For a rising bubble, the change in location with time is a function of the bubble rise velocity, v_b (m s^{-1}), and any associated vertical water velocity, v, and is expressed as

$$\frac{dz}{dt} = v_b + v. \tag{2}$$

[19] Substituting for dt, equation (3) gives the change in moles of gas within the bubble per unit depth (m) as

$$\frac{dM_i}{dz} = -K_{Li}(H_iP_i - C_i)\frac{A_S}{v_b + v}. \tag{3}$$

[20] Bubble size–dependent parameterizations for bubble rise velocity and mass transfer coefficient, as well as a temperature-dependent solubility constant, are listed in Table 1. The above equation is the gas transfer component of the plume model described in section 3.2. The model has been independently validated in discrete-bubble oxygen transfer tests using air bubbles in shallow water (13 m) [*McGinnis and Little*, 2002].

3.2. Bubble-Plume Model

[21] When gas bubbles are released rapidly enough, the resulting local buoyancy increase leads to the upwelling and entrainment of water, thus creating a two-phase plume of water and gas. As the plume rises, the gas bubbles dissolve into the entrained and surrounding water, decreasing the bubble-driven buoyancy. The plume water will lose momentum as the driving force (i.e., bubbles) decreases and as the plume encounters density gradients. When momentum reaches zero, the water will detrain and "fall back" to its equilibrium depth. The density of the plume water is, however, slightly altered because of the increased concentrations of dissolved CO_2 (increases density) or CH_4 (decreases density), and is accounted for in the state equations. Modifying a well-established bubble plume model [*Wüest et al.*, 1992; *McGinnis et al.*, 2004], we investigate the behavior of both CO_2 and CH_4 driven bubble plumes.

[22] The plume model theory and assumptions are detailed by *Wüest et al.* [1992], with the key variables and the associated six simultaneous differential equations given in Table 2 and the range of input values listed in Table 3. The following overview of the model is summarized from *McGinnis et al.* [2004] and *Wüest et al.* [1992]. The model is based on horizontally integrated equations for conservation of mass, momentum, heat, salinity and gases [*McDougall*, 1978]. As the plume rises, water is entrained from the background into the plume proportional to the plume velocity and circumference at depth [*Morton*, 1959]. This entrainment incorporates the boundary effects on the plume due to density and dissolved gas gradients. A key contribution of the *Wüest et al.* [1992] plume model was the variable buoyancy flux resulting from the changing bubble size (section 3.1). *Wüest et al.* [1992] accounted for changing bubble volume due to not only decompression and thermal expansion but also gas dissolution and stripping. Most prior studies neglected gas exchange; however it is particularly important in deep systems or, as in this study, with highly soluble gases (i.e., CO_2) where dissolution is very rapid.

[23] One of the unknowns is the initial water velocity. *Wüest et al.* [1992] suggested using an initial Froude number of 1.6 and solving for the initial velocity where

$$v = Fr\left[2\lambda bg\left(\rho_a - \rho_p\right)/\rho_p\right]^{-1/2}. \tag{4}$$

[24] The major assumptions given by *Wüest et al.* [1992] are summarized here (see Tables 2 and 3 for variable definitions and typical values):

[25] 1. "Top hat" distribution is assumed for velocities, temperature, and undissolved gas concentrations.

[26] 2. All parameters are defined over the plume radius b, except the bubbles which occupy an inner core of the plume given as λb, where $\lambda < 1$ (Table 3).

[27] 3. Gas seepage is assumed to produce bubbles at uniform size and rate, evenly distributed over the source.

[28] 4. Bubbles do not coalesce or break up.

[29] 5. The plume initial properties are the same as at the depth of formation.

Table 1. Gas, Bubble and Water Parameterizations[a]

Equation	Range
$H_O = 2.125 - 5.021 \times 10^{-2}T + 5.77 \times 10^{-4}T^2$ (mol/(m^3 bar))	(T in Celsius)
$H_N = 1.042 - 2.450 \times 10^{-2}T + 3.171 \times 10^{-4}T^2$ (mol/(m^3 bar))	(T in Celsius)
$H_{CH4} = \exp(127.173804 - 155.575631/T \times 100 - 65.2552591 \times LN(T/100) + 6.16975729 \times T/100)$ (Pa)	(T in Kelvin)
$H_{CO2} = \exp(-58.0931 + 90.5069 \times (100/T) + 22.294 \times LN(T/100))/1.01325$ (mol/(L bar))	(T in Kelvin)
$SC = \exp(S \times (0.027766 - 0.025888 \times (T/100) + 0.0050578 \times (T/100)^2))$	(S in PSU) (T in Kelvin)
$K_L = 0.6r$ (m/s)	$r < 6.67 \times 10^{-4}$ m
$K_L = 4 \times 10^{-4}$ (m/s)	$r \geq 6.67 \times 10^{-4}$ m
$v_b = 4474r^{1.357}$ (m/s)	$r < 7 \times 10^{-4}$ m
$v_b = 0.23$ (m/s)	$7 \times 10^{-4} \leq r < 5.1 \times 10^{-3}$ m
$v_b = 4.202r^{0.547}$ (m/s)	$r \geq 5.1 \times 10^{-3}$ m

[a]Modified after *Wüest et al.* [1992] and *McGinnis et al.* [2004].

[30] 6. Entrained water properties are the same as the ambient water at that depth.

[31] 7. No mixing occurs during plume fallback.

[32] 8. Turbulent losses are not considered.

3.3. Parameterizations and Water Density

[33] Parameterizations for the model are obtained mostly from *Wüest et al.* [1992] (Table 1). The salinity effect on solubility, SC, was estimated from *Weiss* [1974]. The Henry's law coefficients for nitrogen and oxygen are the same as used by *Wüest et al.* [1992] and carbon dioxide and methane from *Weiss* [1974] and *Rettich et al.* [1981], respectively. We acknowledge that some of these model parameterizations are simplistic and empirical; however, the model has been validated for an air bubble plume in shallow systems (~45 m) using these values for O_2 and N_2 [*McGinnis et al.*, 2004]. We modified the model to now include CO_2 and CH_4 to simulate the expected behavior of the resulting plumes in the studied systems.

[34] Water density as a function of temperature and salinity is calculated from *Chen and Millero* [1986] for fresh water and from *Intergovernmental Oceanographic Commission* [2010] for seawater. Dissolved methane decreases water density and causes the water to rise [*Linke et al.*, 2010], while dissolved CO_2, like salt, increases the density [*Ohsumi et al.*, 1992; *Schmid et al.*, 2002]. These density contributions are calculated with their respective contraction coefficient as

Table 3. Plume Variables and Initial Conditions

Parameter	Variable	Value
Depth (m)	z	25, 70
Source area (m^2)	π	0.2
Entrainment factor	α	0.11
Plume diameter ratio	λ	0.8
Initial Froude number	Fr	1.6
Source rate (Nm^3/s)	Q_G	1E-6–1
Gas flux (mol/s)	F_G	4.1E-5–41
Initial bubble radius (mm)	r	6

$$\rho(T, S, CO_2, CH_4) = \rho(T, S) \cdot (1 + \beta_{CO2} \cdot CO_2 + \beta_{CH4} \cdot CH_4) \quad (5)$$

where $\beta_{CO2} = 2.84 \times 10^{-4}$ and $\beta_{CH4} = -1.25 \times 10^{-3}$ kg g^{-1} [see *Schmid et al.*, 2002, and references therein].

4. Observations: North Sea Elevated CO_2 Concentrations

[35] High values of CO_2 were measured in the water column at Salt Dome Juist during the October 2008 campaign aboard R/V *Alkor*. During the time of the study the water column was well mixed, with temperatures around 13°C–15°C and salinities at ~34 PSU (Table 4). Average concentrations (and standard deviation) are listed in Table 4. Background gas concentrations were determined from a CTD/water cast at Borkum Reef (CTD 1; Figure 1 and Table 4).

[36] Dissolved oxygen levels were close to saturation around 320 μmol L^{-1}. Methane concentrations were near background values and ranged from 1.9 to 3.2 nmol L^{-1} (about 70%–120%) [*Wiesenburg and Guinasso*, 1979]. Water velocity was measured with the ADCP and was fairly high with ~0.5 m s^{-1} flowing to the WSW around the time of CTD 13. This towed CTD cast delivered the highest measured CO_2 value (discussed below; Figure 2).

[37] The $CO_{2(extr)}$ concentrations were surprisingly high with ~90 (±30, n = 70) μmol L^{-1} measured in bottom waters

Table 2. The Dynamic Variables and the Nonlinear Differential Flux Equations of the Bubble-Plume Model[a]

Variable	Definition	Units
Water volume flux	$Q = \pi b^2 v$	m^3/s
Momentum flux	$M = \pi b^2 v^2$	m^4/s^2
Temperature flux	$F_T = QT_p$	deg C m^3/s
Dissolved solids flux	$F_s = QS\rho_w$	g/s
Dissolved gas fluxes	$F_{Di} = QC_i$	mol/s
Undissolved gas fluxes	$F_{Gi} = \pi b^2 \lambda^2 (v + v_b) y_i$	mol/s
Water volume flux	$\frac{dQ}{dz} = 2\alpha\pi bv$	m^2/s
Momentum flux	$\frac{dM}{dz} = \frac{\rho_a - \rho_p}{\rho_p} g\pi b^2 \lambda^2 + \frac{\rho_a - \rho_w}{\rho_p} g\pi b^2 (1 - \lambda^2)$	m^3/s^2
Temperature flux	$\frac{dF_T}{dz} = 2\alpha\pi bvT_a$	deg C m^2/s
Salinity flux	$\frac{dF_s}{dz} = 2\alpha\pi bv\rho_a S_a$	g/(s m)
Dissolved gas flux	$\frac{dF_{Di}}{dz} = 2\alpha\pi bvC_{ia} + \frac{4\pi r^2 N}{v + v_b} K_L (H_i P_i - C_i)$	mol/(s m)
Undissolved gas flux	$\frac{dF_{Gi}}{dz} = -\frac{4\pi r^2 N}{v + v_b} K_L (H_i P_i - C_i)$	mol/(s m)

[a]Modified after *Wüest et al.* [1992] and *McGinnis et al.* [2004].

Table 4. Results From a Reference Station (CTD 1) and CTDs Collected Over Salt Dome Juist[a]

CTD Profile	Average Depth (m)	Alkalinity (meq/L)	T (deg C)	S (PSU)	$CO_{2(extr.)}$ (μmol/L)	Standard Deviation (μmol/L)	δ^{13} $CO_{2(extr.)}$ (‰PDB)
1	12.0	2.31	15.1	34.5	6.1		−10.2
11	23.7	2.32	13.4	33.3	65.7	15.7	−14.5
12	25.7	2.35	13.2	33.3	82.1	14.2	−13.6
13	11.7	2.35	13.3	33.9	105.8	71.9	−17.0
14	24.4	2.34	13.3	34.0	89.3	8.8	−14.9
15	25.5	2.29	12.9	33.4	85.3	16.2	−14.4
16	23.3	2.33	13.3	34.1	117.2	28.2	−14.1

[a]Results are only for casts where CO_2 was measured. Data were averaged over the sample bottles for each CTD cast (up to 12).

of the Salt Dome Juist area (Figure 2 and Table 4). These values are already substantially elevated by a factor of ~15 over the background concentration of 6 μmol L^{-1}. An exceptionally high value of 318 μmol L^{-1} (~53 times higher than background) was measured in a water sample from 11 m water depth during CTD profile 13 (Figure 2 and Table 4). The δ^{13}C-$CO_{2(extr.)}$ values determined from selected gas samples range between −10.2 and −24 ‰ (Table 4 and Figure 2), whereas the mean value of all δ^{13}C values is about −14.5 ‰ (SD = 2.2, n = 33), suggesting biogenic origin (discussed below).

5. CO_2 and CH_4 Bubble Dynamics

[38] The source and type of CO_2 seepage at Salt Dome Juist are unknown. In the following analyses, we combine simple measurements and modeling of CO_2 bubbles to determine under which conditions bubble release could occur and the potential for acoustic detection. The rate of bubble dissolution in a fluid is largely defined by the local saturation concentration H_iP_i and the concentration of dissolved gas in the surrounding environment C_i, known as the concentration driving force ($H_iP_i - C_i$) (see equation (3)). A review of Henry's coefficients suggest the rapid dissolution of gaseous CO_2 as it is ~25–30 times more soluble in seawater than CH_4 and O_2, and almost 60 times more soluble than N_2 [*Steinmann et al.*, 2008; R. Sander, Compilation of Henry's law constants for inorganic and organic species of potential importance in environmental chemistry (version 3), 1999, available at http://www.henrys-law.org].

5.1. Acoustic Bubble Detection

[39] Methane bubble seepage is relatively simple to detect via hydroacoustics as CH_4 bubbles tend to rise relatively high in the water column because of its low solubility in seawater [*Greinert et al.*, 2006]. In contrast, CO_2 bubbles released in shallow marine environments dissolve much more rapidly. We investigated this experimentally by using an in situ bubble measurement lander in Lake Lucerne. Images of bubbles immediately after being emitted from the bubble orifice were captured from the video. In order to calculate an average diameter of a bubble an elliptical shape is assumed in the first step, and then an equivalent radius is calculated knowing that the actual shape of a rising bubble can change dramatically [*Ostrovsky et al.*, 2008].

[40] Figure 3a shows the tracks produced from CO_2 bubbles with initial measured diameters of 9.7 mm (A), 3.1 mm (B) and 7.8 mm (C). For comparison, Figure 3b shows CH_4 bubbles with initial diameter of 3.0 mm (D) rising compared with the 3.1 mm CO_2 bubble (B). Figure 3b clearly shows that the rise velocity from the CO_2 bubble is much slower than the CH_4 bubble (Figure 3c). As rise velocity is a function of bubble size [*Haberman and Morton*, 1954], we can deduce that the CO_2 bubble (B) dissolved much more rapidly, and must be quite small by the time it is "seen" by the sonar. Bubbles with diameters of 2–10 mm rise at around 22–25 cm s^{-1}. Below 2 mm, the bubble rise velocity drastically drops so that the bubble with a rise velocity of 7 cm s^{-1} must be around 0.6 mm in diameter (see bubble velocity equation in Table 1). This was also visually confirmed when the bubble lander was brought toward the surface and bubbles were released about 1.5 m below the water surface.

[41] These observations agree very well with the model results using the solubility constant reported for CO_2 by *Weiss* [1974]. Both the rapid and preferential dissolution

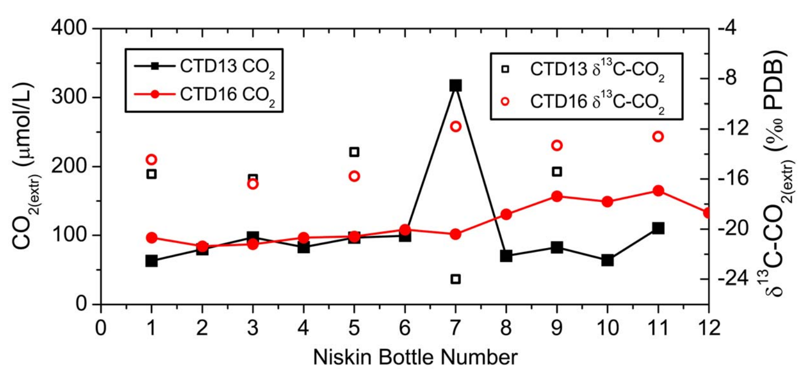

Figure 2. Results from CTDs 13 and 16 over Salt Dome Juist showing isotope data and concentrations of extracted CO_2. Atmospheric equilibrium CO_2 concentration is 6 μmol/L.

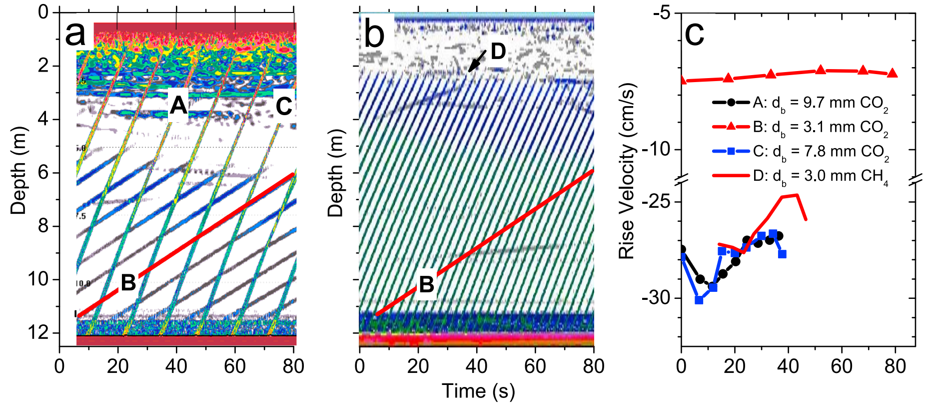

Figure 3. Results of acoustic bubble detection experiment in Lake Lucerne. (a) Hydrograph of CO_2 released from ~13 m deep. Initial bubble diameters, d, producing the shown acoustic tracks are d = 9.7 mm for track A, d = 3.1 mm for track B, and d = 7.8 mm for track C. (b) Acoustic tracks from a 3.0 mm diameter released CH_4 bubble (D). For comparison, the 3.1 mm diameter CO_2 bubble track (shown in red in Figure 3a) is overlaid in red. (c) Bubble rise velocities for the shown tracks. Using Figure 7 from *McGinnis et al.* [2006], we are able to determine that the 3.1 mm CO_2 bubble must be ~0.6 mm by the time it appears in the sonar image, which means that the bubble diameter shrank by 2.6 mm within 1.3 m distance from the bottom.

of CO_2 (compared to N_2) was also reported by *White et al.* [2006]. We did attempt to calibrate the model using these measurements; however, this was proven to be difficult as the gas composition of CO_2 bubbles forming on the nozzle changed too rapidly, and results are highly sensitive to the initial mole fraction of CO_2 (discussed below). Therefore a more sophisticated modeling approach is needed that includes gas transport during the time of bubble growth and formation at the nozzle, or a method of producing CO_2 bubbles that do not remain on the nozzle during formation for any length of time.

5.2. Implications

[42] The fact that CO_2 bubbles released in shallow waters dissolve very rapidly presents complications with respect to their detection. For example, Figure 4a is the ADCP backscatter at the time CTD 13 measured the highest CO_2 concentrations, in which the backscatter shows persistent high signals at the bottom starting at ~25 m. Figure 4b also shows the results from the bubble model for CO_2 bubbles (solid lines) with 4, 6, and 8 mm initial diameters demonstrating that the bubbles mostly dissolved within the first 1–3 m upon release. The backscatter signal drastically decreases between 21 and 23 m depth, and almost entirely disappears at 17 m, a range that corresponds with the modeled dissolution of CO_2 bubbles. Therefore, it is not possible to determine if the high backscatter at the seafloor indicates CO_2 bubble release or is due to entrained sediment as a result of rough weather during sampling or a combination of both. Further modeling results presented below suggest that the bubble release scenario is unlikely and that the backscatter is likely attributed to resuspended sediment.

[43] The rapid dissolution rate of the CO_2 bubble becomes more obvious when compared with that of CH_4 (Figure 4b). The methane bubbles reach the surface with ease and remain the same or even increase in volume as they rise. These bubbles are therefore much more easily detectable with hydroacoustic technology. As shown in Figure 4b, as the diameter of the CO_2 bubbles decrease to ~1 mm (depending on initial size), the rate of dissolution becomes much slower. As the CO_2 is being dissolved, other dissolved gasses are stripped from the water column into the bubble (Figure 4c). When nearly all the CO_2 in a bubble is dissolved, the gasses that were previously stripped (N_2 and O_2) begin to redissolve. Note that after CO_2 is dissolved from the bubble, the O_2 and N_2 mole fractions approach atmospheric levels (Figure 4c), while the CH_4 bubble is still around 80%–90% methane at 10 m depth.

5.3. CO_2 Bubbles in Sediment

[44] We evaluated the dissolution rate of a hypothetical stationary bubble as if it would have instantly appeared, e.g., in the sediment pore water (Figure 5). For this basic modeling exercise we assumed that there is no dissolved gas accumulation in the pore water (assumed saturated levels of O_2 and N_2), and that any gas that is transferred from the bubble to the dissolved phase is instantly carried away. This model simulation was performed at 20°C and 35 PSU.

[45] Figures 5a and 5b illustrate the change in the mole fraction over time. As seen in the case of our 3 mm bubble, the mole fraction approaches 0.5 for CO_2 in less than 3 s. This does not include the time when the bubble is growing, e.g., on the nozzle, as in the case of our bubble release experiment. The CO_2 is almost completely gone within 4 s for the 3 mm bubble and about 6 s for the 6 mm bubble.

[46] The 6 mm CO_2 bubble "lifetime" in our hypothetical gas-depleted pore water would only last for about 10 s. The lifetime of the CH_4 bubble would be about 300 s (30 times longer) and the N_2 bubble would be 700 s (70 times longer), which scales to the Henry's coefficients. These results suggest that unless there is a strong and persistent source of CO_2, it is very unlikely that there would be small-scale CO_2 bubble seepage as is commonly observed at CH_4 bubble seeps. As discussed later, the pore water concentrations of CO_2 would have to approach 100 mmol L^{-1} for small-scale seepage to occur.

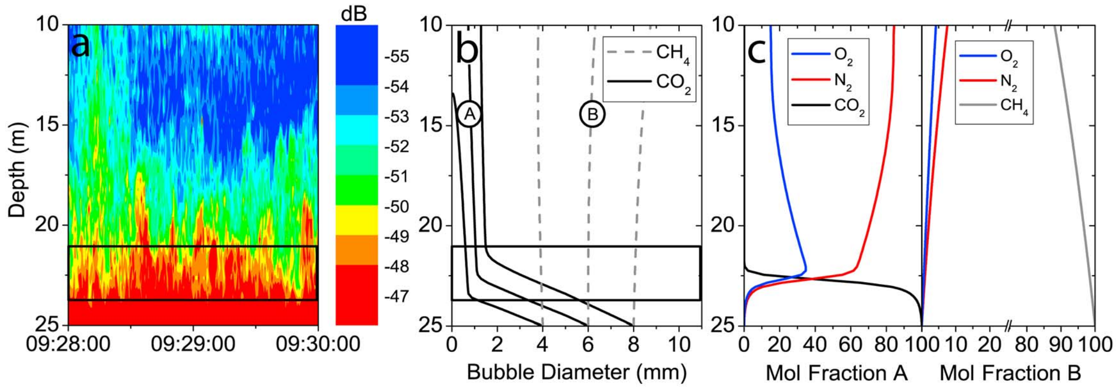

Figure 4. (a) ADCP backscatter showing bottom "flares" (red signal) at Salt Dome Juist. (b) Bubble modeling results for pure CO_2 bubbles (solid lines) and pure CH_4 bubbles (dashed lines) emerging with 4, 6, and 8 mm diameter from the seafloor showing the changing diameter with depth. (c) The evolution of gaseous mole fractions for the 6 mm CO_2 (fraction A) and CH_4 (fraction B) bubbles shown in Figure 4b.

5.4. Comparing CO_2 and CH_4 Plumes

[47] The difference between the dissolution rates of CO_2 bubbles versus CH_4 bubbles obviously will have a large impact on the buoyancy of the plume. We performed plume model simulations for both CO_2 and CH_4 bubbles released from A) a deep stratified, and B) shallow well-mixed water columns (Table 3). For the shallow runs we assume the initial conditions present at Salt Dome Juist during the October 2008 cruise (CTD 1; Table 4), and for the deep summer stratified case we used conditions from a profile at Tommeliten (Figure 6a), a 70 m deep site in the central North Sea.

[48] Plume model runs were conducted with mass flux rates (gas input) shown in Table 3. Results are shown in Figure 6. The initial velocities are solved for using an initial Froude number of 1.6 in equation (4). For a given depth, the initial velocity is independent of the gas used as long as the gas density is approximately the same (Figure 6b).

[49] Figure 6c shows the final plume concentrations when it falls back to the density equilibrium depth. As expected, the CO_2 plumes include generally higher CO_2 concentrations due to the much more rapidly dissolving bubbles. The plume typically stops and the water "peels" away even though bubbles are still present. These bubbles could go on to create secondary plumes.

[50] Figure 6d shows the depth of maximum plume rise (solid symbols), and the fall back (detrained water equilibrium) depth (open symbols). In the shallow case, the CO_2 plume does not rise very high with the lower gas inputs. This is because the CO_2 completely dissolves and the plume does not receive as much buoyancy as does the CH_4 plume. The CH_4 plume, however, reaches the surface every time. Not shown here are the fall back depths. In every case, the CH_4 plume remains at the surface because of the slightly decreased density imparted by the dissolved CH_4 concentrations. Conversely, the

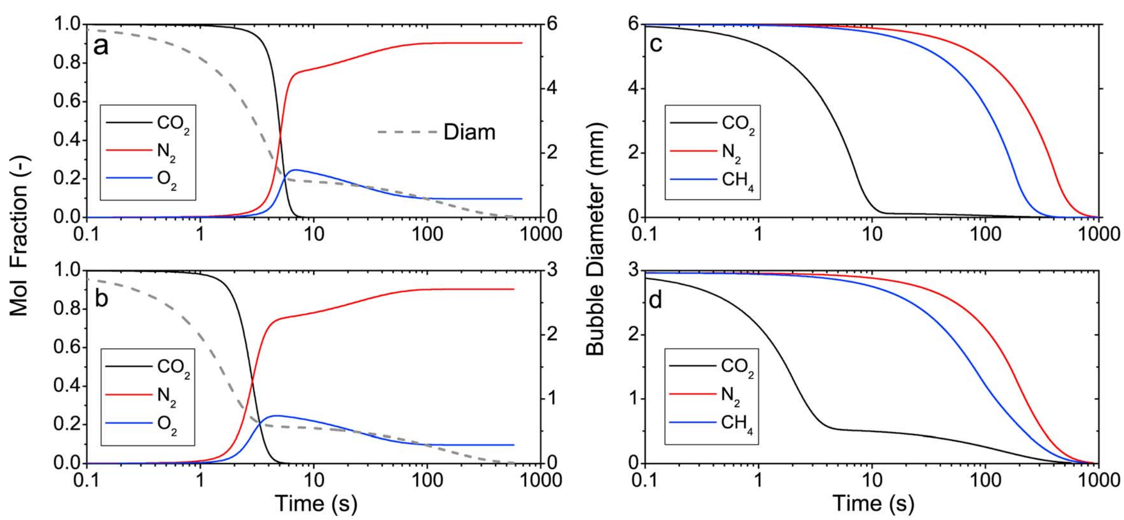

Figure 5. Theoretical evolution of mole fraction of CO_2, N_2, and O_2 bubbles and bubble diameter over time (blue) for (a) a stationary 6 mm diameter bubble and (b) a 3 mm diameter bubble in the sediment (assuming no accumulation of dissolved gases). Bubble diameter over time for CO_2, N_2 and CH_4 (c) 6 mm and (d) 3 mm bubbles in the sediment.

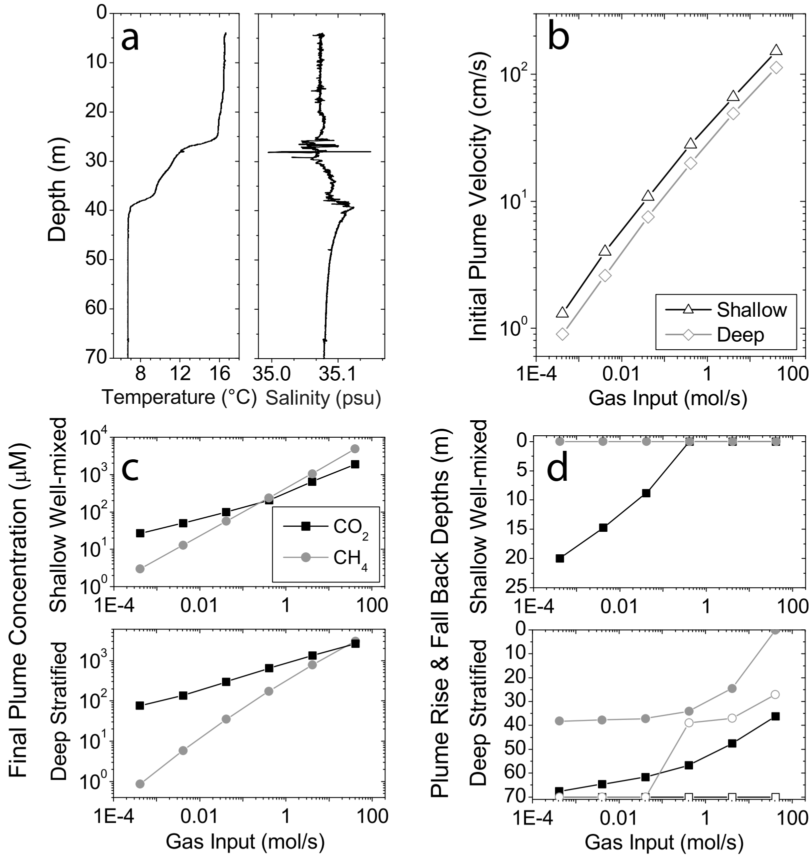

Figure 6. (a) Boundary conditions for stratified runs. Data are obtained from the Tommeliten site. (b) Initial plume velocity for shallow (Salt Dome Juist) and deep (Tommeliten) cases as a function of molar gas input from seepage. (c) Expected concentration of plume when it reaches final equilibrium depth after rise and potential fall back. (d) Depths of maximum plume rise (solid symbols) and "fall back" equilibrium (open symbols) as a function of molar gas input from seepage.

CO_2 plume water will fall completely back to the seafloor (this assumes no mixing for the downwelling plume water).

[51] For the deeper, stratified conditions shown in Figure 6a, the CO_2 plume barely rises for the lower flow rates (closed squares) and then falls back to the seafloor (open squares). The rise height is even less due to the slight bottom stratification and the decreased volume flux as a result of the release depth increase. The CH_4 plume, however, makes it to the bottom of the thermocline even at lower fluxes (or inputs). Eventually with the high flux of 41 mol s^{-1} (58 t d^{-1}), the plume finally penetrates through the thermocline and reaches the surface.

[52] Our highest measured CO_2 value was 300 μmol L^{-1}. If we assume that this is a plume-generated source, it would correspond to a CO_2 input of 1 mol s^{-1} (nearly 4 t d^{-1}) and a final plume diameter of 14 m (area = 150 m^2), which is substantial. If this was indeed a plume, then this would be a conservative estimate of source strength as it likely would have been considerably diluted when we obtained the measurement.

6. CO_2 in the North Sea

6.1. Thermodynamic Calculations

[53] $CO_{2(aq)}$ equilibrium concentrations were estimated to be between 6 and 13 μmol L^{-1} (T = 15°C, pH = 8.2–8.4, Alk = 2.4 meq L^{-1}) [*Pierrot et al.*, 2006]. This is in the range of gaseous CO_2 extracted from water samples from station CTD 1 (Background station; Table 4). A calculated value of about 200–300 ppm (CO_2 in dry atmosphere) would reflect a CO_2 sink compared to, for example, 370 ppm CO_2 in the atmosphere.

[54] The high CO_2 concentration of 318 μmol L^{-1} measured from CTD 13–7 (Figure 2) had a pH of 6.8 ± 0.2. A pH value of 6.8 corresponds to calculated values of about 9000 ppm CO_2 in dry air and a $CO_{2(aq)}$ value of about 320 μmol L^{-1}. Slight reduction of pH in North Sea waters has been seen where respiration takes place, and annual cycles of pH vary between 7.8 and 8.4 depending on the distance to the coast [*Blackford and Gilbert*, 2007]. On the basis of measured data and box modeling, *Blackford and Gilbert* [2007] determined riverine inflow, respiration, and benthic or pelagic processes as the main reasons for reduced pH values in the North Sea. Obviously our measured pH value of 6.8 would require a much stronger CO_2 input.

6.2. Origin of the CO_2

[55] CH_4 oxidation in the water column is not the source for high CO_2 concentrations as only background methane concentrations reflecting equilibrium with atmospheric methane were observed (data not shown). Moreover, methane concentrations are orders of magnitude (~2–3 μmol L^{-1}) lower than $CO_{2(extr.)}$ and they did not vary significantly with CO_2 concentrations.

[56] The negative $\delta^{13}C$-CO_2 values indicate a dominant biogenic source in the working area. The most negative $\delta^{13}C$ value (−24‰; Figure 2) is related to the highest CO_2 concentration. Consequently, it is assumed that the carbon of the seeping CO_2 mainly originates from degradation of organic matter or methane oxidation within the sediment [*Whiticar and Faber*, 1986; *Mook and Tan*, 1991]. Considering the isotope fractionation at laboratory temperatures between $CO_2(g)$-$CO_2(aq)$ of ~1‰ and $CO_2(aq)$-HCO_3^- of about −10‰ [*Chacko et al.*, 2001], sample CTD 1 reflects normal North Sea water conditions [*Mook and Tan*, 1991] and sample CTD 13 a mixed fluid. Therefore, it is difficult to determine the exact fluid origin (i.e., the benthic layer, Holocene peat deposits, or even deeper strata) that serves as a CO_2 source [e.g., *del Giorgio and Williams*, 2005; *Fischer et al.*, 2006; *Steinmann et al.*, 2008].

6.3. Pathways, Fate, and Potential Detection of CO_2 Seepage

[57] We have found evidence of CO_2 seepage, although the source and mechanism are still unclear. Using a simple modeling approach we suggest that bubbles were unlikely to be present under the prevailing conditions at Salt Dome Juist during the R/V *Alkor* cruise. Bubble formation would only occur when the solubility of gases (i.e., CO_2) in seawater is exceeded. For the actual seafloor conditions at Salt Dome Juist (T~290 K, S~35‰, 20 m depth) about 100 mmol L^{-1} CO_2 is calculated as CO_2 solubility after *Duan and Sun* [2003] and *Duan et al.* [2006], which would imply a pH value of ~4.3 in the fluid and sediment. Such a significantly acidic pH is far lower than the pH range measured for high respiratory shelf sediment [*Zhu et al.*, 2006] and would therefore open the discussion for additional, perhaps deep-seated CO_2 sources.

[58] The bubble plume modeling did not rule out such a plume source; however, it would likely be a single phase plume (i.e., only liquid) with no bubbles (free gas). A buoyant enough point source with inputs ranging from roughly 1–10 t d^{-1} is needed to explain the observed strong CO_2 signal. Such a buoyancy source driving the plume could be a (1) slightly elevated seepage temperature, (2) fresher groundwater input, or (3) strong hydrostatic head (perhaps driven from onshore rain events). We would like to note that during a return cruise aboard R/V *Celtic Explorer* in August 2009 the seep could not be relocated. This would suggest (not surprisingly) that it is an intermittent, and perhaps seasonal, source.

[59] Even without bubbles, CO_2 entering the water column from the sediment at Salt Dome Juist will reach the atmosphere. This is due to the well-mixed, shallow water column and surface mass transfer. However, for the stratified summer deep (70 m) situation, any potential CO_2 bubbles and plume would stop at the thermocline, thus trapping the CO_2 in the bottom water. This CO_2 could reach the atmosphere during the fall turnover, which may help explain the CO_2 flux increases reported by *Bozec et al.* [2005], or be transported and sequestered within the North Atlantic Ocean deep waters as suggested by *Thomas et al.* [2004].

[60] The results of this study have implications and present challenges for the detection of CO_2 seepage at shallow CCS sites:

[61] 1. Significant seepage of CO_2 is necessary for CO_2 bubbles to be present.

[62] 2. Even if CO_2 bubbles are present, they are hard to detect because of rapid dissolution.

[63] 3. CO_2 bubble-driven plumes would not rise as high in the water column as would CH_4 bubble-driven plumes and tend to fall back farther.

[64] 4. CO_2 adds density, and thus monitoring and sampling should be concentrated at the seafloor.

[65] 5. CH_4 bubbles could be sought out as precursors or indicators of potential CO_2 seepage.

Notation

A area, m^2.
b plume radius, m.
C dissolved concentration, mol m^{-3}.
d bubble diameter, mm.
F_D dissolved species flux, mol s^{-1}.
F_G gaseous species flux, mol s^{-1}.
Fr Froude number, dimensionless.
F_S salinity flux, g s^{-1}.
F_T temperature flux, °C m^3 s^{-1}.
g gravitational acceleration, m s^{-2}.
K_L mass transfer coefficient, m s^{-1}.
M plume momentum, m^4 s^{-2}.
N number flux of bubbles, s^{-1}.
P pressure, bar.
Q plume flow rate, m^3 s^{-1}.
r bubble radius, m.
S salinity, g kg^{-1}.
SC salinity correction, PSU.
t time, s.
T temperature, °C.
v velocity, m s^{-1}.
y gaseous concentration, mol m^{-3}.
z depth, m.

Greek letters
α entrainment coefficient, dimensionless.
β density contraction coefficients, kg g^{-1}.
λ ratio of bubble-containing region of plume.
ρ density, kg m^{-3}.
s surface.

Subscripts
a ambient water.
b bubble.
I gas species.
p plume water and gas mixture.
w plume water.

[66] **Acknowledgments.** Many thanks to the captain and crew of R/V *Alkor*. We are grateful for the technical support of Uwe Koy, Thorsten Schott, and Christian do Santos Ferreira and the analytical work of Anke Bleyer, Markus Faulhaber, and Jakob Wanke. Financial support was provided by the Wintershall AG. Peter Eisenach and Bert Clever provided important geological and geophysical background information and data. Thanks to Christian Dinkel at Eawag for assistance in collecting bubble data and to the three reviewers for their very helpful suggestions.

References

Ague, J. J. (2000), Release of CO_2 from carbonate rocks during regional metamorphism of lithologically heterogeneous crust, *Geology*, *28*(12), 1123–1126, doi:10.1130/0091-7613(2000)28<1123:ROCFCR>2.0.CO;2.

Alendal, G., and H. Drange (2001), Two-phase, near-field modeling of purposefully released CO_2 in the ocean, *J. Geophys. Res.*, *106*(C1), 1085–1096, doi:10.1029/1999JC000290.

Berner, R. A. (1980), *Early Diagenesis: A Theoretical Approach*, 241 pp., Princeton Univ. Press, Princeton, N. J.

Blackford, J. C., and F. J. Gilbert (2007), pH variability and CO_2 induced acidification in the North Sea, *J. Mar. Syst.*, *64*, 229–241, doi:10.1016/j.jmarsys.2006.03.016.

Blackford, J. C., N. Jones, R. Proctor, and J. Holt (2008), Regional scale impacts of distinct CO_2 additions in the North Sea, *Mar. Pollut. Bull.*, *56*, 1461–1468, doi:10.1016/j.marpolbul.2008.04.048.

Bozec, Y., H. Thomas, K. Elkalay, and H. J. W. de Baar (2005), The continental shelf pump for CO_2 in the North Sea—Evidence from summer observation, *Mar. Chem.*, *93*, 131–147, doi:10.1016/j.marchem.2004.07.006.

Caldeira, K., and M. E. Wickett (2005), Ocean model predictions of chemistry changes from carbon dioxide emissions to the atmosphere and ocean, *J. Geophys. Res.*, *110*, C09S04, doi:10.1029/2004JC002671.

Cathles, L. M., Z. Su, and D. Chen (2010), The physics of gas chimney and pockmark formation, with implications for assessment of seafloor hazards and gas sequestration, *Mar. Pet. Geol.*, *27*, 82–91, doi:10.1016/j.marpetgeo.2009.09.010.

Chacko, T., D. R. Cole, and J. Horita (2001), Equilibrium oxygen, hydrogen and carbon isotope fractionation factors applicable to geological systems, in *Stable Isotope Geochemistry*, *Rev. Mineral. Geochem.*, vol. 43, edited by J. W. Valley and D. Cole, pp. 1–81, doi:10.213Ch8/gsrmg.43.1.1, Mineral. Soc. of Am., Washington, D. C.

Chen, C. A., and F. J. Millero (1986), Precise thermodynamic properties for natural waters covering only the limnological range, *Limnol. Oceanogr.*, *31*, 657–662, doi:10.4319/lo.1986.31.3.0657.

Dando, P. R., et al. (2000), Hydrothermal studies in the Aegean Sea, *Phys. Chem. Earth*, *25*, 1–8, doi:10.1016/S1464-1909(99)00112-4.

del Giorgio, P. A., and P. Williams (2005), *Respiration in Aquatic Ecosystems*, 326 pp., doi:10.1093/acprof:oso/9780198527084.001.0001, Oxford Univ. Press, New York.

Dimitrov, L. I. (2003), Mud volcanoes—A significant source of atmospheric methane, *Geo Mar. Lett.*, *23*, 155–161, doi:10.1007/s00367-003-0140-3.

Duan, Z. H., and R. Sun (2003), An improved model calculating CO_2 solubility in pure water and aqueous NaCl solutions from 273 to 533 K and from 0 to 2000 bar, *Chem. Geol.*, *193*(3–4), 257–271, doi:10.1016/S0009-2541(02)00263-2.

Duan, Z. H., R. Sun, C. Zhu, and I.-M. Chou (2006), An improved model for the calculation of CO_2 solubility in aqueous solutions containing Na^+, K^+, Ca^{2+}, Mg^{2+}, Cl^-, and SO_4^{2-}, *Mar. Chem.*, *98*, 131–139, doi:10.1016/j.marchem.2005.09.001.

Ehlers, J. (1990), Reconstructing the dynamics of the north-west European Pleistocene ice sheets, *Quat. Sci. Rev.*, *9*, 71–83, doi:10.1016/0277-3791(90)90005-U.

Esposito, A., G. Giordano, and M. Anzidei (2006), The 2002–2003 submarine gas eruption at Panarea volcano (Aeolian Islands, Italy): Volcanology of the seafloor and implications for the hazard scenario, *Mar. Geol.*, *227*, 119–134, doi:10.1016/j.margeo.2005.11.007.

Fischer, M., R. Botz, M. Schmidt, K. Rockenbauch, D. Garbe-Schönberg, J. Glodny, P. Gerling, and R. Littke (2006), Origins of CO_2 in Permian carbonate reservoir rocks (Zechstein, Ca2) of the NW-German Basin (Lower Saxony), *Chem. Geol.*, *227*, 184–213, doi:10.1016/j.chemgeo.2005.09.014.

Foote, K. G., H. P. Knudsen, G. Vestnes, D. N. MacLennon, and E. J. Simmonds (1987), Calibration of acoustic instruments for fish density estimation: A practical guide, *ICES Coop. Res. Rep. 144*, 57 pp., Int. Counc. for the Explor. of the Sea, Copenhagen.

Friedrich, T., and A. Oschlies (2009), Basin-scale pCO_2 maps estimated from ARGO float data: A model study, *J. Geophys. Res.*, *114*, C10012, doi:10.1029/2009JC005322.

Greinert, J., Y. Artemov, V. Egorov, M. De Batist, and D. McGinnis (2006), 1300-m-high rising bubbles from mud volcanoes at 2080 m in the Black Sea: Hydroacoustic characteristics and temporal variability, *Earth Planet. Sci. Lett.*, *244*, 1–15, doi:10.1016/j.epsl.2006.02.011.

Haberman, W. L., and R. K. Morton (1954), An experimental study of bubbles moving in liquids, *Proc. Am. Soc. Civ. Eng.*, *80*, 379–427.

Hall-Spencer, J. M., R. Rodolfo-Metalpa, S. Martin, E. Ransome, M. Fine, S. M. Turner, S. J. Rowley, D. Tedesco, and M.-C. Buia (2008), Volcanic carbon dioxide vents show ecosystem effects on ocean acidification, *Nature*, *454*, 96–99, doi:10.1038/nature07051.

Haszeldine, R. S. (2009), Carbon capture and storage: How green can black be?, *Science*, *325*, 1647–1652, doi:10.1126/science.1172246.

Haugan, P. M., and F. Joos (2004), Metrics to assess the mitigation of global warming by carbon capture and storage in the ocean and in geological reservoirs, *Geophys. Res. Lett.*, *31*, L18202, doi:10.1029/2004GL020295.

Haugan, P. M., F. Thorkildsen, and G. Alendal (1995), Dissolution of CO_2 in the ocean, *Energy Convers. Manage.*, *36*, 461–466, doi:10.1016/0196-8904(95)00044-E.

Holloway, S., J. M. Pearce, V. L. Hards, T. Oshumi, and J. Gale (2007), Natural emissions of CO_2 from the geosphere and their bearing on the geological storage of carbon dioxide, *Energy*, *32*, 1194–1201, doi:10.1016/j.energy.2006.09.001.

Huuse, M., and H. Lykke-Andersen (2000), Overdeepened Quaternary valleys in the eastern Danish North Sea: Morphology and origin, *Quat. Sci. Rev.*, *19*, 1233–1253, doi:10.1016/S0277-3791(99)00103-1.

Intergovernmental Oceanographic Commission (2010), *The International Thermodynamic Equation of Seawater—2010: Calculation and Use of Thermodynamic Properties, Manuals Guides 56*, 196 pp., U. N. Educ., Sci. and Cult. Organ., Paris.

Intergovernmental Panel on Climatic Change (IPCC) (2007), Summary for policymakers, in *Climate Change 2007: Impacts, Adaptation and Vulnerability: Contribution of Working Group II to the Fourth Assessment Report of the Intergovernmental Panel on Climate Change*, edited by M. L. Parry et al., pp. 7–22, Cambridge Univ. Press, Cambridge, U. K.

Italiano, F., and P. M. Nuccio (1991), Geochemical investigations of submarine volcanic exhalations to the east of Panarea, Aeolian Islands, Italy, *J. Volcanol. Geotherm. Res.*, *46*, 125–141, doi:10.1016/0377-0273(91)90079-F.

Judd, A. G., and M. Hovland (2007), *Seabed Fluid Flow: The Impact on Geology, Biology, and the Marine Environment*, 475 pp., doi:10.1017/CBO9780511535918, Cambridge Univ. Press, New York.

Keir, R. S., J. Greinert, M. Rhein, G. Petrick, J. Sültenfuß, and K. Fürhaupter (2005), Methane and methane carbon isotope ratios in the northeast Atlantic including the Mid-Atlantic Ridge (50°N), *Deep Sea Res., Part I*, *52*(6), 1043–1070, doi:10.1016/j.dsr.2004.12.006.

Keir, R. S., O. Schmale, M. Walter, J. Sültenfuß, R. Seifert, and M. Rhein (2008), Flux and dispersion of gases from the "Drachenschlund" hydrothermal vent at 8°18′S, 13°30′W, *Earth Planet. Sci. Lett.*, *270*, 338–348, doi:10.1016/j.epsl.2008.03.054.

Keir, R. S., O. Schmale, R. Seifert, and J. Sultenfuss (2009), Isotope fractionation and mixing in methane plumes from the Logatchev hydrothermal field, *Geochem. Geophys. Geosyst.*, *10*, Q05005, doi:10.1029/2009GC002403.

Kennett, J. P., K. G. Cannariato, I. L. Hendy, and R. J. Behl (2003), *Methane Hydrates in Quaternary Climate Change: The Clathrate Gun Hypothesis*, *Spec. Publ. Ser.*, vol. 54, 216 pp., AGU, Washington, D. C.

Kharaka, Y. K., D. R. Cole, S. D. Hovorka, W. D. Gunter, K. G. Knauss, and B. M. Freifeld (2006), Gas-water-rock interactions in Frio Formation following CO_2 injection: Implications for the storage of greenhouse gases in sedimentary basins, *Geology*, *34*(7), 577–580, doi:10.1130/G22357.1.

Leifer, I., and R. K. Patro (2002), The bubble mechanism for methane transport from the shallow sea bed to the surface: A review and sensitivity study, *Cont. Shelf Res.*, *22*, 2409–2428, doi:10.1016/S0278-4343(02)00065-1.

Lenton, T. M., and M. G. R. Cannel (2002), Mitigating the rate and extent of global warming, *Clim. Change*, *52*(3), 255–262, doi:10.1023/A:1017483501347.

Lewicki, J. L., J. T. Birkholzer, and C.-F. Tsang (2007), Natural and industrial analogues for leakage of CO_2 from storage reservoirs: Identification of features, events, and processes and lessons learned, *Environ. Geol.*, *52*(3), 457–467, doi:10.1007/s00254-006-0479-7.

Linke, P., S. Sommer, L. Rovelli, and D. F. McGinnis (2010), Physical limitations of dissolved methane fluxes: The role of bottom-boundary layer processes, *Mar. Geol.*, *272*, 209–222, doi:10.1016/j.margeo.2009.03.020.

Lokhorst, A. (1998), *NW European Gas Atlas: Composition and Isotope Ratios of Natural Gases* [CD-ROM], Neth. Inst. of Appl. Geosci. (TNO), Haarlem, Netherlands.

Lupton, J., et al. (2006), Submarine venting of liquid carbon dioxide on a Mariana Arc volcano, *Geochem. Geophys. Geosyst.*, *7*, Q08007, doi:10.1029/2005GC001152.

McDougall, T. J. (1978), Bubble plumes in stratified environments, *J. Fluid Mech.*, *85*, 655–672, doi:10.1017/S0022112078000841.

McGinnis, D. F., and J. C. Little (2002), Predicting diffused-bubble oxygen transfer rate using the discrete-bubble model, *Water Res.*, *36*, 4627–4635, doi:10.1016/S0043-1354(02)00175-6.

McGinnis, D. F., A. Lorke, A. Wüest, A. Stöckli, and J. C. Little (2004), Interaction between a bubble plume and the near field in a stratified lake, *Water Resour. Res.*, *40*, W10206, doi:10.1029/2004WR003038.

McGinnis, D. F., J. Greinert, Y. Artemov, S. E. Beaubien, and A. Wüest (2006), Fate of rising methane bubbles in stratified waters: How much methane reaches the atmosphere?, *J. Geophys. Res.*, *111*, C09007, doi:10.1029/2005JC003183.

Mook, W. G., and F. C. Tan (1991), Stable carbon isotopes in rivers and estuaries, in *Biogeochemistry of Major World Rivers, SCOPE 42*, edited by E. T. Degans, S. Kempe, and J. E. Richey, pp. 245–264, John Wiley, Chichester, N. Y.

Morton, B. R. (1959), Forced plumes, *J. Fluid Mech.*, *5*, 151–163, doi:10.1017/S002211205900012X.

Ohsumi, T., N. Nakashiki, K. Shitashima, and K. Hirama (1992), Density change of water due to dissolution of carbon dioxide and near-field behavior of CO_2 from a source on deep-sea floor, *Energy Convers. Manage.*, *33*, 685–690, doi:10.1016/0196-8904(92)90072-5.

Orr, F. M., Jr. (2009), Onshore geologic storage of CO_2, *Science*, *325*, 1656–1658, doi:10.1126/science.1175677.

Orr, J. C., et al. (2005), Anthropogenic ocean acidification over the twenty-first century and its impact on calcifying organisms, *Nature*, *437*, 681–686, doi:10.1038/nature04095.

Ostrovsky, I., D. F. McGinnis, L. Lapidus, and W. Eckert (2008), Quantifying gas ebullition with an echosounder: The role of methane transport by bubbles in a medium-sized lake, *Limnol. Oceanogr. Methods*, *6*, 105–118.

Pierrot, D., E. Lewis, and D. W. R. Wallace (2006), MS Excel program developed for CO2 system calculation, *ORNL/CDIAC-105a*, 21 pp., Carbon Dioxide Inf. Anal. Cent., Oak Ridge Natl. Lab., Oak Ridge, Tenn.

Prowe, A. E. F., H. Thomas, J. Pätsch, W. Kühn, Y. Bozec, L.-S. Schiettecatte, A. V. Borges, and H. J. W. de Baar (2009), Mechanisms controlling the air-sea CO_2 flux in the North Sea, *Cont. Shelf Res.*, *29*, 1801–1808, doi:10.1016/j.csr.2009.06.003.

Reeburgh, W. S. (2003), Global methane biogeochemistry, in *Treatise on Geochemistry*, vol. 4, *The Atmosphere*, edited by H. D. Holland and K. K. Turekian, pp. 65–89, Elsevier, Oxford, U. K.

Reeburgh, W. S. (2007), Oceanic methane biogeochemistry, *Chem. Rev.*, *107*, 486–513, doi:10.1021/cr050362v.

Rettich, T. R., Y. P. Handa, R. Battino, and E. Wilhelm (1981), Solubility of gases and liquids: 13. High-precision determination of Henry's constants for methane and ethane in liquid water at 275 to 328 K, *J. Phys. Chem.*, *85*, 3230–3237, doi:10.1021/j150622a006.

Sabine, C. L., et al. (2004), The ocean sink for anthropogenic CO_2, *Science*, *305*, 367–371, doi:10.1126/science.1097403.

Schmid, M., K. Tietze, M. Halbwachs, A. Lorke, D. McGinnis, and A. Wüest (2002), How hazardous is the gas accumulation in Lake Kivu? Arguments for a risk assessment in light of the Nyiragongo Volcano eruption of 2002, *Acta Vulcanol.*, *14*(1–2), 115–122.

Schneider von Deimling, J., J. Greinert, N. R. Chapman, W. Rabbel, and P. Linke (2010), Acoustic imaging of natural gas seepage in the North Sea: Sensing bubbles controlled by variable currents, *Limnol. Oceanogr. Methods*, *8*, 155–171, doi:10.4319/lom.2010.8.155.

Schrag, D. P. (2009), Storage of carbon dioxide in offshore sediments, *Science*, *325*, 1658–1659, doi:10.1126/science.1175750.

Schroot, B. M., and R. T. E. Schüttenhelm (2003), Shallow gas and gas seepage: Expressions on seismic and other acoustic data from the Netherlands North Sea, *J. Geochem. Explor.*, *78–79*, 305–309, doi:10.1016/S0375-6742(03)00112-2.

Siegenthaler, U., and J. L. Sarmiento (1993), Atmospheric carbon dioxide and the ocean, *Nature*, *365*, 119–125, doi:10.1038/365119a0.

Steinmann, P., B. Eilrich, M. Leuenberger, and S. J. Burns (2008), Stable carbon isotope composition and concentrations of CO_2 and CH_4 in the deep catotelm of a peat bog, *Geochim. Cosmochim. Acta*, *72*, 6015–6026, doi:10.1016/j.gca.2008.09.024.

Streif, H. (2002), Nordsee und Küstenlandschaft-Beispiel einer dynamischen Landschaftsentwicklung, in *Natur und Landschaft Zwischen Küste und Harz*, vol. 20, pp. 134–149, Akad. für Geowiss. und Geotech., Hannover, Germany.

Thomas, H., Y. Bozec, K. Elkalay, and H. J. W. de Baar (2004), Enhanced open ocean storage of CO_2 from shelf sea pumping, *Science*, *304*, 1005–1008, doi:10.1126/science.1095491.

Thomas, H., et al. (2007), Rapid decline of the CO_2 buffering capacity in the North Sea and implications for the North Atlantic Ocean, *Global Biogeochem. Cycles*, *21*, GB4001, doi:10.1029/2006GB002825.

Tivey, M. K., A. M. Bradley, T. M. Joyce, and D. Kadko (2002), Insights into tide-related variability at seafloor hydrothermal vents from time-series temperature measurements, *Earth Planet. Sci. Lett.*, *202*, 693–707, doi:10.1016/S0012-821X(02)00801-4.

Usdowski, E., and J. Hoefs (1990), Kinetic $^{13}C/^{12}C$ and $^{18}O/^{16}O$ effects upon dissolution and outgassing of CO_2 in the system CO_2-H_2O, *Chem. Geol.*, *80*, 109–118.

Veron, J. E. N., O. Hoegh-Guldberg, T. M. Lenton, J. M. Lough, D. O. Obura, P. Pearce-Kelly, C. R. C. Sheppard, M. Spalding, M. G. Stafford-Smith, and A. D. Rogers (2009), The coral reef crisis: The critical importance of <350 ppm CO_2, *Mar. Pollut. Bull.*, *58*, 1428–1436, doi:10.1016/j.marpolbul.2009.09.009.

Weiss, R. F. (1974), Carbon dioxide in water and seawater: The solubility of a non-ideal gas, *Mar. Chem.*, *2*, 203–215, doi:10.1016/0304-4203(74)90015-2.

White, S. N., P. G. Brewer, and E. T. Peltzer (2006), Determination of gas bubble fractionation rates in the deep ocean by laser Raman spectroscopy, *Mar. Chem.*, *99*, 12–23, doi:10.1016/j.marchem.2004.10.006.

Whiticar, M. J., and E. Faber (1986), Methane oxidation in sediment and water column environments—Isotope evidence, *Adv. Org. Geochem.*, *10*, 759–768, doi:10.1016/S0146-6380(86)80013-4.

Wiesenburg, D. A., and N. L. Guinasso Jr. (1979), Equilibrium solubilities of methane, carbon monoxide, and hydrogen in water and sea water, *J. Chem. Eng. Data*, *24*(4), 356–360, doi:10.1021/je60083a006.

Wüest, A., N. H. Brooks, and D. M. Imboden (1992), Bubble plume modeling for lake restoration, *Water Resour. Res.*, *28*(12), 3235–3250, doi:10.1029/92WR01681.

Zhu, Q. Z., R. C. Aller, and Y. Z. Fan (2006), Two-dimensional pH distributions and dynamics in bioturbated marine sediments, *Geochim. Cosmochim. Acta*, *70*, 4933–4949, doi:10.1016/j.gca.2006.07.033.

T. DelSontro, Surface Waters—Research and Management, Eawag: Swiss Federal Institute of Aquatic Science and Technology, Seestrasse 79, CH-6047 Kastanienbaum, Switzerland.

P. Linke, D. F. McGinnis, A. Reitz, L. Rovelli, and M. Schmidt, Leibniz Institute of Marine Sciences at University of Kiel (IFM-GEOMAR), East Shore Campus, Wischhofstrasse 1-3, D-24148 Kiel, Germany. (dmcginnis@ifm-geomar.de)

S. Themann, Sedimentology, Coastal- and Continental Shelf Research, Institute of Geosciences, University of Kiel, Otto-Hahn-Platz 1, D-24118 Kiel, Germany.